JACS
JOURNAL OF THE AMERICAN CHEMICAL SOCIETY
Article
pubs.acs.org/JACS

Enzymatic Synthesis of Periodic DNA Nanoribbons for Intracellular pH Sensing and Gene Silencing

Gang Chen,† Di Liu,† Chunbai He,† Theodore R. Gannett, Wenbin Lin, and Yossi Weizmann*

Department of Chemistry, The University of Chicago, 929 East 57th Street, Chicago, Illinois 60637, United States

Supporting Information

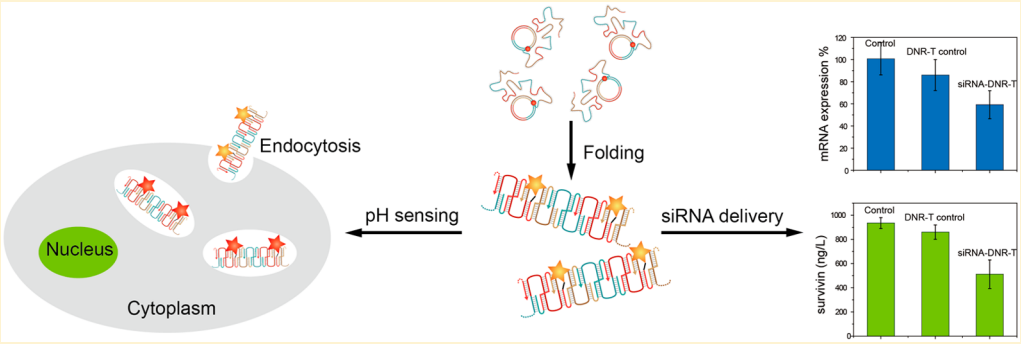

ABSTRACT: We report the construction of periodic DNA nanoribbons (DNRs) by a modified DNA origami method. Unlike the conventional DNA origami, the DNR scaffold is a long, single-stranded DNA of tandem repeats, originating from the rolling circular amplification (RCA). Consequently, the number of folding staple strands tremendously decreases from hundreds to a few, which makes the DNR production scalable and cost-effective, thus potentially removing the barrier for practical applications of DNA nanostructures. Moreover, the co-replicational synthesis of scaffold and staple strands by RCA-based enzymatic reactions allows the generation of DNRs in one pot, further reducing the cost. Due to their unique periodicity, rigidity, and high aspect ratio, DNRs are efficiently internalized into cells and escape from endosomal entrapment, making them potential nanocarriers for imaging agents and biological therapeutics. We demonstrated proof-of-concept applications of DNRs as an intracellular pH sensor and an efficient small interfering RNA delivery vehicle in human cancer cells.

INTRODUCTION

In the past three decades, DNA, the genetic material, has evolved as powerful building blocks for constructing complex artificial nanostructures through programmed self-assembly.[1−5] In particular, the advent of DNA origami strategy has allowed the folding of a long single-stranded DNA (ssDNA) scaffold into arbitrary two- and three-dimensional nanoarchitectures,[6−10] unveiling a new scenario for addressable positioning of nano- and/or biomaterials.[11−17] The compact DNA origami structures render them resistant to nuclease degradation and thus remain functional in cell lysates.[18] In addition, the biocompatibility and efficient cellular uptake of self-assembled DNA nanostructures make them promising candidates for cellular imaging[19,20] and delivery applications.[21−23]

Nearly all scaffold strands for DNA origami are virus genomes and need to be folded by hundreds of short synthetic oligonucleotide staple strands. Despite the elegant and exquisite shape control, the conventional DNA origami production is time-intensive and cost-ineffective because of the complicated structure design, the limited availability of scaffolds, and the need for hundreds of staple strands. These limitations have thus far made large-scale production of DNA origami a formidable challenge, which hinders their exploration for potential biomedical applications, such as the selective delivery of imaging and therapeutic agents. To overcome this hurdle, elegant strategies have been developed for DNA origami production by utilizing the scaffold or staple strands obtained by enzymatic reactions[24,25] or by constructing periodic structures with reduced staple strands.[26,27]

Here we show the construction of periodic DNA nanoribbon (DNR) structures by using the rolling circle amplification (RCA) product as scaffold which is folded by only three short staple strands or one concatenated long staple strand. As an isothermal enzymatic DNA replication process, RCA yields long ssDNA with tandem repeats of the sequence complementary to the circular ssDNA template.[28] Since each repeat in the RCA product can be folded by the same set of staple strands, one-dimensional periodic structure is easily generated. This DNR design is inspired by natural one-dimensional structures with high aspect ratio, such as actin filaments and microtubules, which have a multitude of functions in organism. Besides scaffold strand, we demonstrate that the concatenated staple strand could also be synthesized by integrating RCA and nicking processes. This co-replicational synthesis of scaffold and staple strands allows the generation of a DNR in one pot. The

Received: December 12, 2014
Published: January 26, 2015

DOI: 10.1021/ja512665z
J. Am. Chem. Soc. 2015, 137, 3844−3851

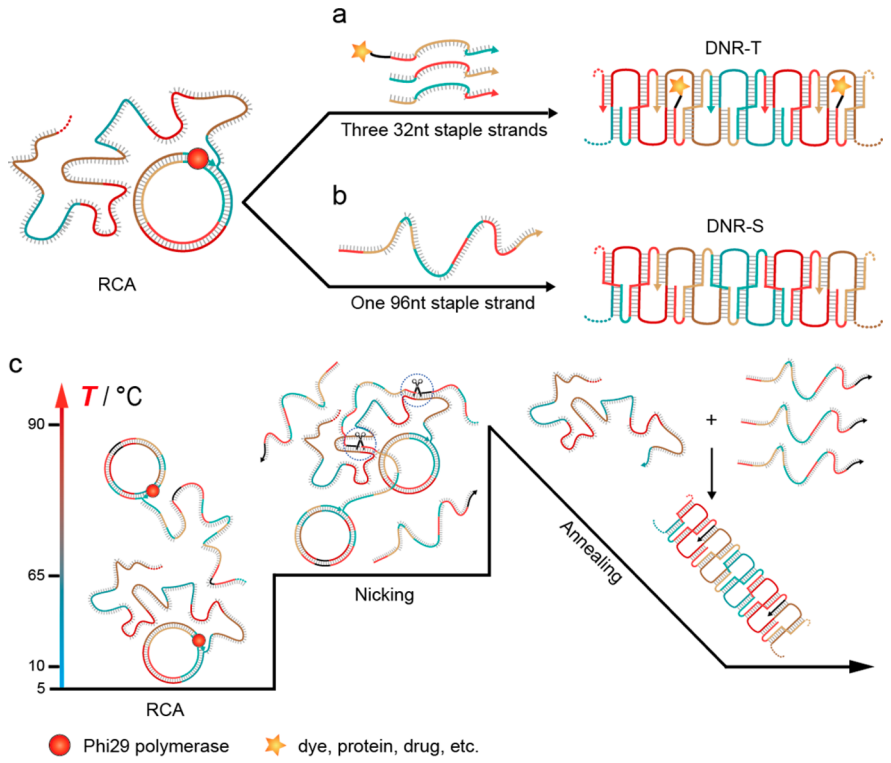

Figure 1. Schematic representation of the enzymatic synthesis of DNR structures. (a) DNR-T structures assembled from RCA scaffold strand and three 32-nt staple strands. (b) DNR-S structures assembled from RCA scaffold strand and one synthetic 96-nt staple strand. (c) Generation of DNR nanostructure by enzymatic reactions in one pot.

ribbon-like shape and rigidity of DNR will allow its efficient penetration through the plasma membrane, where the shape effects have been demonstrated in other artificial delivery systems, such as polymer filaments[29] and carbon nanotubes.[30,31] In the proof-of-concept experiments, we loaded this periodic DNR with biologic and synthetic cargoes at high capacities, including streptavidin, fluorescence dyes, and small interfering RNA (siRNA). We showed that functionalized DNRs could be efficiently internalized into cells, recruit endosomes, and escape from endosomal entrapment. We demonstrated that DNRs represent a novel class of nanocarriers for intracellular pH sensing with the loaded fluorescein dye and for effective gene silencing in human cancer cells with the conjugated siRNA targeting survivin, respectively.

EXPERIMENTAL SECTION

Design and Formation of DNR Structures from RCA Scaffold and Synthetic Staple Strands. Sequence design was carried out with the programs CANADA version 2.0 and NUPACK. Enzymatic ligation of RCA templates was performed by T4 DNA Ligase. After RCA with Phi29 DNA polymerase, the products were purified using Nanosep centrifugal devices (MWCO 100 K). All oligonucleotides were quantified by measuring OD_{260} with the extinction coefficient ε260 calculated with IDT's OligoAnalyzer. The RCA product and commercial staple strands were combined with various molecular ratios in a TAE/Mg^{2+} buffer and slowly cooled from 90 to 10 °C. After annealing, the samples were imaged by AFM in air at room temperature.

One-Pot Enzymatic Generation of DNR. Two circular ssDNA templates (RCA scaffold template and RCA staple template), which had been annealed with their primers, were mixed together and incubated with Phi29 DNA polymerase and Nb.BsmI nicking enzyme at 5 °C for 4 h in 1× TAE/Mg^{2+} buffer. Then, the reaction temperature was increased to 65 °C and held for 12 h for the completion of the nicking process. The temperature was then increased to 90 °C and slowly cooled to 10 °C. The samples were purified by Nanosep centrifugal devices (MWCO 100 K).

AFM Imaging of DNR. A 5 μL sample was pipetted on a freshly cleaved mica (Ted Pella, Inc.) and left to absorb for 1.5 min. Then, the surface was washed 3 times by 20 μL of purified water and gently blown dry by nitrogen gas. The prepared samples were scanned by ScanAsyst-air tips in ScanAsyst Imaging Mode on Multimode 8 Atomic Force Microscope with a NanoScope V controller (Bruker Inc.).

Intracellular pH Sensing in H460 Cells. Five hundred thousands of H460 cells were seeded on a glass-bottom Petri dish (no. 1.5, coated with poly lysine, MatTek Corporation) and further cultured for 24 h after which the cell culture medium was removed and replaced with fresh HBSS. The cells were incubated with FAM-DNR-T for 5, 10, 20, and 30 min, respectively, and fixed with 4% paraformaldehyde. The cells were imaged using Leica SP5 II microscope equipped with 100×, 1.4 oil objective, PMT fluorescence detector, and transmitted light detector with DIC polarizer. For pH measurements, cells were imaged in three channels to yield three images, (i) exciting at 488 nm and collecting at 520 nm, (ii) exciting at 435 nm and collecting at 520 nm, and (iii) DIC. Mean intensity of endosomes was measured in 488 and 435 nm channels, and a ratio of 488 to 435 nm intensities was obtained. pH was calculated from the pH calibration curve obtained with buffer solutions.

Gene Silencing in SKOV-3 Cells. Human ovarian cancer cell SKOV-3 were seeded on 24-well plate at 1×10^4 cells/well and further cultured for 24 h. The culture media was changed to serum-free McCoy's 5A and siRNA-DNR-T was added to the cells at a siRNA dose of 30 nM for a 4 h incubation. Upon discarding the serum-free culture media, the cells were further cultured for 20 h in serum-containing media. The supernatant of culture media was collected and analyzed by ELISA (R&D Systems, USA) to quantify the extracellular surivin production. RNA from the transfected cells was extracted using the Trizol reagent protocol (Invitrogen, USA). From 500 ng of total RNA, cDNA was synthesized using PrimeScriptRT reagent kit (Takara

DOI: 10.1021/ja512665z
J. Am. Chem. Soc. 2015, 137, 3844−3851

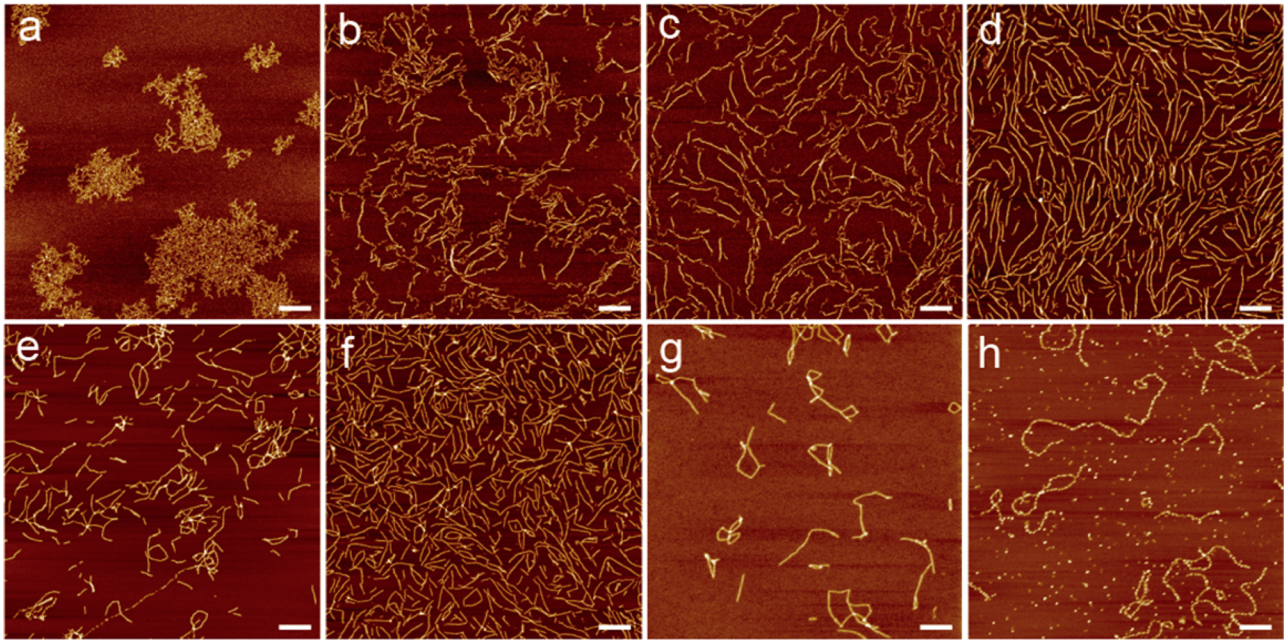

Figure 2. AFM characterization of DNR structures. (a) RCA product without staple strands. (b–d) DNR-T structures at different staple-to-scaffold ratios, 3:1 (b), 10:1 (c), and 100:1 (d). (e,f) DNR-S structures at different staple-to-scaffold ratios, 3:1 (e) and 10:1 (f). (g) DNR structures generated by autonomous enzymatic reaction in one-pot. (h) Directed assembly of streptavidin linear arrays on dual-biotin modified DNR-T surface. Bar = 200 nm.

Biotechnology Co. Ltd.). Synthesized cDNA, forward and reverse primers, as well as the SYBR Premix Ex Taq (Takara Biotechnology Co. Ltd.) were run on the CFX96 Real-Time PCR Detection System (Bio-Rad, USA) for the determination of cellular survivin mRNA level. Sequences of the primers used were designed with Primer Bank (Table S1). β-actin serves as an internal control.

RESULTS

DNR Formation. We first designed the DNR with three staple stands (DNR-T). It consists of repeated rectangular units of six parallel helical domains, with each domain containing a 16 bp segment of DNA helix (Figure 1a and Scheme S1). In each rectangular unit, three nicked helical domains are separated by the unnicked domain along the extension direction. The nicks are placed in such a way that each rectangular unit contains one continuous long strand (scaffold strand) and three 32-nt short strands (staple strands). The scaffold contains tandem 96-nt repeats, which is the RCA product of a 96-nt-long circularized template. Each staple strand has a 16-nt segment in the center and an 8-nt segment on the ends. This design enables the hierarchical assembly of DNR-T in a one-step annealing process. As the temperature drops, the central 16-nt segment of each staple is the first part to hybridize to the scaffold, forming the unnicked domain. Once the staple strands bind to the scaffold through intermolecular base-pairing interactions, all further interactions required for DNR assembly are intramolecular hybridizations between the 8-nt end segments of the staple strand and scaffold to form nicked domains. The intramolecular hybridization process is expected to be more efficient than the competing intermolecular interactions that may cause undesirable cross-linking and aggregation between individual nanoribbons. This strategy of hierarchical interaction has been utilized by Turberfield and co-workers to build the DNA tetrahedron[32] and is a ubiquitous feature in DNA origami staple designs.[6−8] Each domain contains 1.5 turns of DNA helix, ensuring that the scaffold strand enters and exits each helical domain at the opposite sides, thereby keeping the whole structure in one plane. The designed rectangular unit has a finite size of ∼13.5 nm in length (2.25 nm width of each double helix in DNA origami nanostructures)[8] and ∼5.4 nm in width (length of the 1.5 turns of helix of B-DNA). Extension of these rectangular units forms the periodic DNR-T structure.

The formation of DNR was confirmed by atomic force microscopy (AFM) imaging. Annealed without staple strands, the RCA scaffold appeared as random coils of ssDNA on the mica surface (Figure 2a). Once annealed with three 32-nt staple strands, the RCA scaffold strand was organized and changed from random coils to one-dimensional nanostructures (Figures 2b–d, S2, and S3). At a low staple-to-scaffold ratio (1:1 or 3:1), the scaffold strand was unraveled and partially folded into organized nanostructures by the staple strands at some locations along the scaffold (Figures 2b and S2). The compacted and organized sections were separated by loose and unorganized sections, which could be distinguished by their heights determined by AFM. When the ratio was increased to 10:1, the organized sections became dominant throughout the structure with only a small portion of defects (Figure 2c). Furthermore, at a ratio of 100:1, a well-organized, one-dimensional nanoribbon structure was observed with very few defects (Figure 2d). Control experiments showed that all three staple strands were necessary to correctly fold the scaffold, while only one or two staple strands failed (Figure S4).

The thermal stability of the DNR-T structure was evaluated by fluorescence-based thermal denaturation assay (Figure S5).[33] Melting curve and its negative first derivative showed two major melting temperatures (T_m) of 59.4 and 62.0 °C, which were slightly higher than those (55.1 and 57.4 °C) calculated for the 16 bp domains in the DNR-T structure.

One-Pot Enzymatic Generation of DNR. In the DNR-T, the 3′ end of each staple strand meets the 5′ end of another staple strand, making it possible to concatenate them into one

DOI: 10.1021/ja512665z
J. Am. Chem. Soc. 2015, 137, 3844−3851

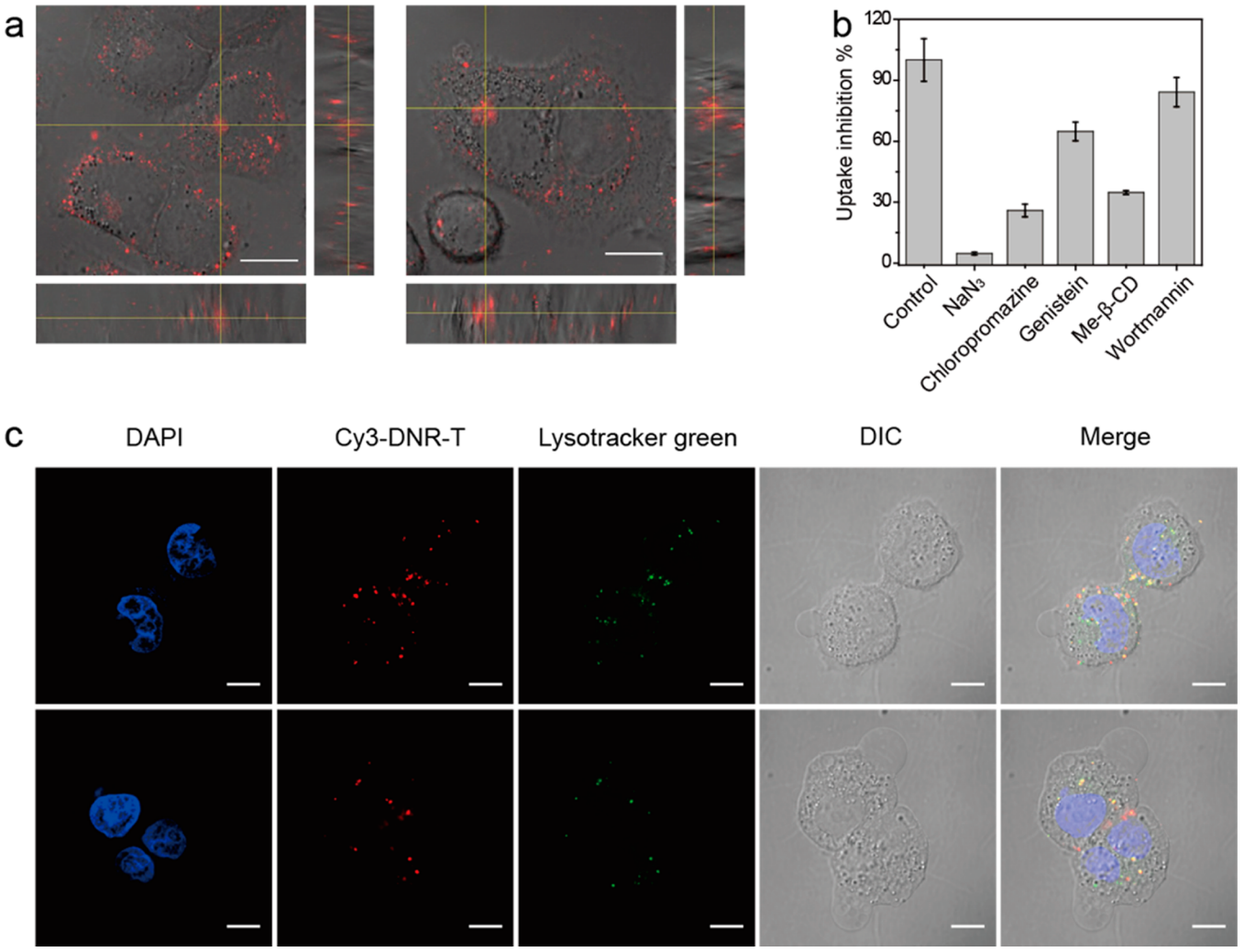

Figure 3. Cellular uptake of DNR structure and its endocytosis pathway. (a) Orthogonal views showing the intracellular distribution of Cy3-DNR-T after incubating with H460 cells for 30 min. Bar = 10 μm. (b) Uptake inhibition of Cy3-DNR-T in H460 cells preincubated with different uptake inhibitors including chlorpromazine (10 μg/mL, clathrin-mediated endocytosis inhibitor), genistein (200 μg/mL, caveolae-mediated endocytosis inhibitor), methyl-β-cyclodextrin (Me-β-CD, 50 μM, lipid-raft-mediated endocytosis inhibitor), wortmannin (50 nM, macropinocytosis inhibitor), and NaN3 (10 mM, energy-dependent endocytosis inhibitor). Results were expressed as the percentage uptake of the control upon incubation with Cy3-DNR-T at 37 °C for 4 h. Data are presented as means ± SD (n = 3). (c) CLSM images showing the endosomal escape of Cy3-DNR-T in H460 cells. The cells were incubated with Cy3-DNR-T for 2 h, fixed with 4% paraformaldehyde, and stained with DAPI and Lysotracker Green to visualize the nuclei and endosomes, respectively. The separation of red (Cy3-DNR-T) and green (Lysotracker Green labeled endosomes) indicated the successful endosomal escape of Cy3-DNR-T. Bar = 10 μm.

staple strand to reduce the number of staples even further. Therefore, we used the RCA product as the scaffold and only one synthetic staple (96-nt) to create DNR-S structure (Figure 1b and Scheme S2). The morphologies of the different structures with variable staple-to-scaffold ratios were analyzed by AFM imaging (Figures 2e,f and S6). As the 96-nt staple strand yielded a well-organized DNR structure, we used RCA to produce a second long strand with tandem repeats of the 96-nt staple unit (RCA staple strand) and incorporated a nicking recognition site on this strand to allow a nicking enzyme to cleave the RCA staple strand into 96-nt staple strands (Scheme S3). To eliminate the use of synthetic complementary strands necessary for the nicking reaction, we utilized the hybridization between RCA scaffold and RCA staple strands. We chose the nicking enzyme Nb.BsmI with the optimum temperature of 65 °C and designed one of the six 16-bp domains containing the nicking recognition site with a T_m of 65 °C, which is higher than the other 16-bp domains (~55 °C). This design weakened the hybridization of the other domains at the nicking stage, while keeping the domain containing the nicking recognition site as stable duplex to facilitate the nicking reaction. As the nicking efficiency relied on the hybridization between the two RCA strands, the ratio of RCA staple strand to RCA scaffold strand and the reaction temperature were optimized to be 1:1 and 65 °C, respectively (Figure S8). As the staple strands were also synthesized by enzymatic reactions,[34] we expected that both scaffold and staple strands could be synthesized in one pot to create a DNR structure.

To realize one-pot enzymatic generation of DNR, we devised a simple process involving three thermal stages in one closed tube containing the components essential for the RCA and nicking reactions (Figure 1c and Scheme S4): (i) RCA generated the scaffold and staple strands (with tandem repeats of the staple sequence); (ii) nicking enzyme cleaved the RCA staple strand into its monomeric units; and (iii) final annealing process completed the production of DNR. Through this

DOI: 10.1021/ja512665z
J. Am. Chem. Soc. 2015, 137, 3844−3851

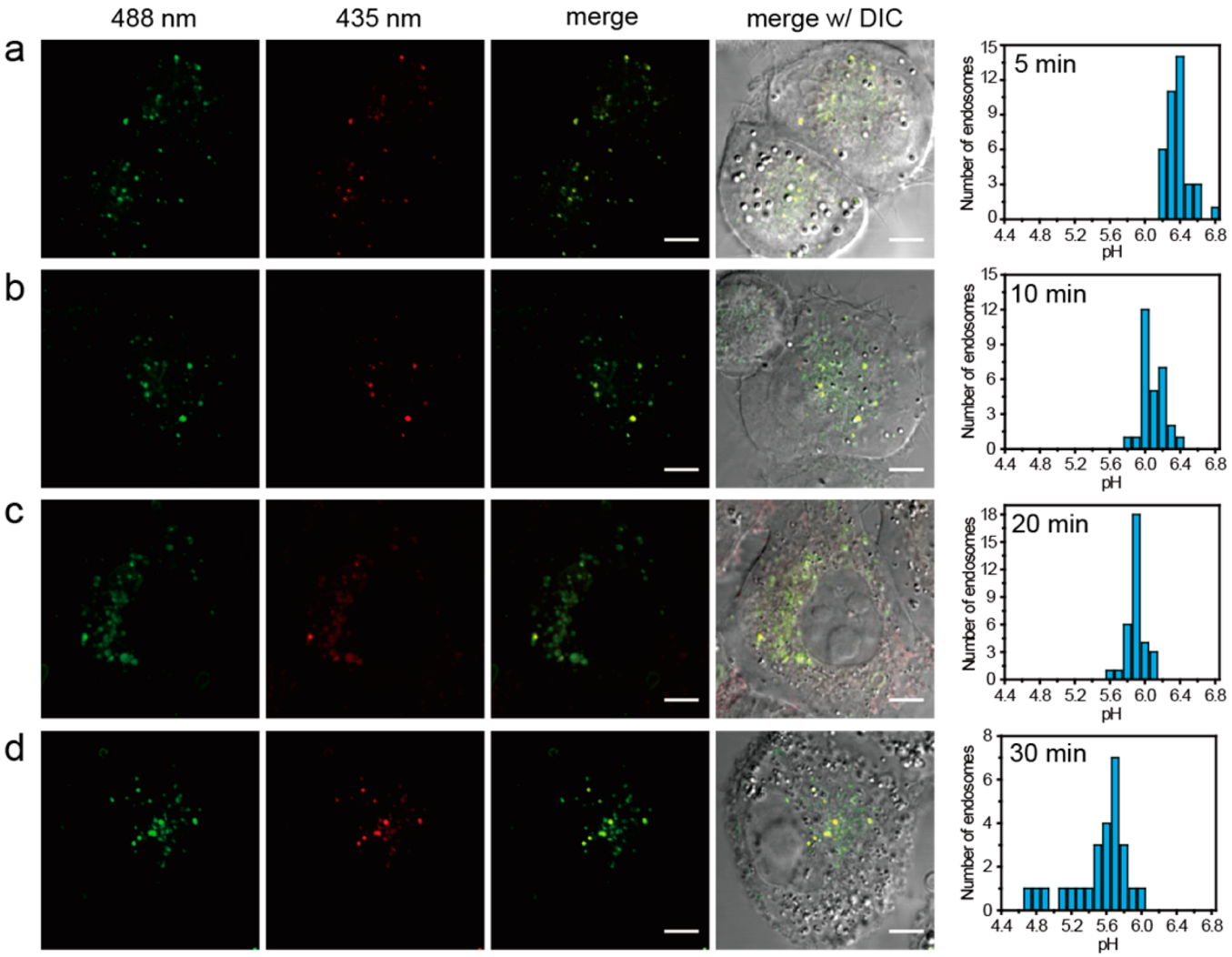

Figure 4. Intracellular pH sensing by FAM-DNR-T. H460 cells were incubated with FAM-DNR-T for different times and imaged with CLSM after fixation, (a) 5, (b) 10, (c) 20, and (d) 30 min. The CLSM images were acquired with a 488 nm laser (green), a 435 nm laser (red), and DIC, respectively. Bar = 5 μm. The histogram shows the number of endosomes at different pH's.

simple and programmable process, one-dimensional DNR was successfully generated (Figure 2g). The results were consistent with those of the DNR-S that were constructed using synthetic 96-nt staple strands (Figure S6).

Cargo Loading onto DNRs. Assembled DNA arrays provide excellent templates for addressable and programmable positioning of other objects.[11,14,35] To show the DNR-T as an efficient delivery vehicle, one of the three 32-nt staple strands was modified with dual biotins at the 5′ end, and streptavidin was then employed as a model cargo. After annealing, the biotin-modified DNR-T had the same morphology as the unmodified one in AFM (Figure S12). However, when it was incubated with streptavidin overnight at 4 °C, periodical bumps were observed on the DNR-T surface, indicating the successful incorporation of the streptavidin (Figure 2h). The measured height of the bumps was ∼3 nm, higher than the ∼1.5 nm measured for the biotin-modified DNR-T (Figure S12). The measured distance between each pair of adjacent bumps was ∼14 nm, matching the length of designed rectangular repeating unit of the DNR-T. The uniformity of the periodic bumps in the linear array, which resulted from the binding of streptavidin, suggested that DNR-T could act as a potential delivery vehicle with a high loading capacity of 45.7 wt %.

Cellular Uptake of DNR-T. To explore the cellular uptake of DNR-T, Cy3 labeled staple was used to construct Cy3-DNR-T, which shared similar morphology with original DNR-T as evidenced by AFM (Figure S13). The cellular internalization of Cy3-DNR-T was evaluated by live cell imaging (Supporting Video). As shown in the video, Cy3-DNR-T rapidly adhered to the cell membrane upon addition to the cell culture medium, followed by translocation to the cytoplasm with part of the Cy3-DNR-T distributed close to the nuclei within 20 min. Orthogonal view images confirmed that the Cy3-DNR-T was efficiently internalized by the cells rather than just adhered to the cell membrane (Figure 3a). By preincubating the cells with a series of inhibitors to block specific internalization pathway, we demonstrated that the cellular internalization of Cy3-DNR-T was not via macropinocytosis but via clathrin- and lipid raft-mediated endocytosis (Figure 3b). This result indicated that Cy3-DNR-T would experience the endo/lysosomal pathway upon entering the cells. Further we investigated the interactions between Cy3-DNR-T and endosomes. Interestingly, the endosome clusters (green fluorescence) significantly colocalized with Cy3-DNR-T (red fluorescence) after incubating Cy3-DNR-T with H460 cells for 30 min, suggesting that the Cy3-DNR-T might be able to recruit endosomes (Figure S14). This

DOI: 10.1021/ja512665z
J. Am. Chem. Soc. 2015, 137, 3844−3851

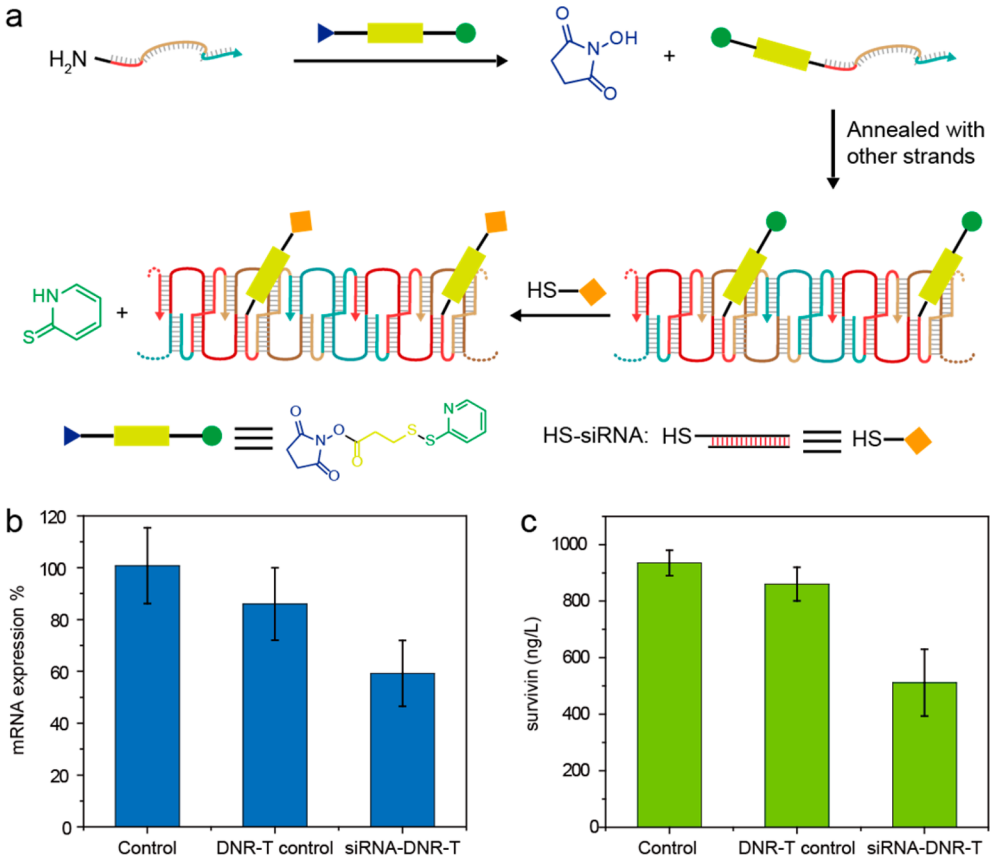

Figure 5. Gene silencing mediated by siRNA-DNR-T. (a) Schematic illustration of the linkage of the siRNA to DNR-T structure. siRNA-DNR-T effectively decreased the survivin mRNA expression (b) and survivin protein production (c) at a siRNA dose of 30 nM in SKOV-3 cells, which were determined by realtime PCR and ELISA assay, respectively. siRNA-DNR-T significantly suppressed the mRNA expression and protein production of survivin with a P value of 0.0206 and 0.0044, respectively, compared to the control by two-tail t test. DNR-T control mediated inappreciable knockdown of mRNA expression and protein production of survivin with a P value of 0.2743 and 0.1572, respectively, compared to the control by two-tail t test.

result could be attributed to their rigid "nanoribbon" structure with high aspect ratio[29] that might cross-link the endosomes. Cy3-DNR-T also showed abilities to escape from the endosomal entrapment, as suggested by the separation of red fluorescence (Cy3-DNR-T) and green fluorescence (Lysotracker Green) in the cells incubating with Cy3-DNR-T for 2 h (Figure 3c).

pH Sensing with DNR-T. Inspired by the efficient endocytosis of DNR-T, we conjugated a fluorescein derivative dye, carboxyfluorescein (FAM), to one of the staple strands. FAM is a pH-sensitive dye that exhibits pH-dependent ratiometric fluorescence changes and, therefore, can be utilized to probe the intracellular pH.[36,37] The periodicity and rigidity of DNR-T could effectively prevent the fluorescence quenching resulting from the dye aggregation and retain favorable fluorescence efficiency with a FAM loading of 0.6 wt %. Ratiometric pH-sensitivity of FAM-DNR-T was first determined in Hanks' balanced salt solution (HBSS) with a pH range from 4.0 to 8.0 by confocal laser scanning microscopy (CLSM). By exciting FAM at 488 and 435 nm and measuring the fluorescence response at 520 nm, a calibration curve was generated (Figure S15). The pH response of FAM-DNR-T exhibited high sensitivity and relatively small deviations at pH > 5.0, indicating the potential application of FAM-DNR-T in sensing intracellular pH. We then performed the measurements of intracellular pH on fixed cells that had been incubated with FAM-DNR-T for 5, 10, 20, and 30 min. After incubation, the pH values of endosome in cells were obtained from the calibration curve based on the CLSM measurements. The histograms showed the number distribution of endosomes of different pHs (Figure 4). The endosome acidification evolved overtime with pH decreasing from 6.4 to 5.6 in 30 min, which is in agreement with previous reports of endosome maturation processes.[38] FAM-DNR-T thus exhibits desired pH response sensitivity, providing a reliable and accurate method for sensing intracellular pH.

siRNA Delivery by DNR-T. As a result of its rigid structure and high aspect ratio, DNR-T is able to escape from endosomal entrapment without involving a proton pump. Therefore, we hypothesized that DNR-T could be exploited as an effective siRNA delivery vehicle for mediating gene silencing without relying on a cationic transfection agent.[39] Survivin has been identified as one member of the inhibitor-of-apoptosis family and is highly expressed in most human tumors, which provides one possibility for cancer therapy through down-regulating survivin expression to increase cancer cell apoptosis.[40,41] We herein chose siRNA targeting survivin as a model and conjugated it to the SPDP-modified staple strand of DNR-T through thiol exchange (Figure 5a and Supporting Information). siRNA-DNR-T achieved a high siRNA loading of 18.3 wt %. DNR control was prepared by mixing siRNA with DNR-T in the absence of SPDP linker (see Supporting Information).

DOI: 10.1021/ja512665z
J. Am. Chem. Soc. 2015, 137, 3844−3851

The *in vitro* gene silencing mediated by siRNA-DNR-T in human ovarian cancer cells SKOV-3 was carried out at a siRNA dose of 30 nM and with a total transfection time of 24 h. The RNAi efficiency was determined by realtime PCR for the quantification of mRNA expression and enzyme-linked immunosorbent assay (ELISA) for the quantification of protein production. As shown in Figure 5, siRNA-DNR-T effectively down-regulated the survivin mRNA expression and protein production by 40.8 ± 12.7% and 45.2 ± 12.6%, respectively; while DNR control showed unappreciable gene silencing effect. Our results suggest that siRNA-DNR-T provides an efficient means for delivering siRNA to cytoplasm without involving the proton sponge mechanism and effectively mediates gene silencing in human cancer cells.

■ DISCUSSION AND CONCLUSION

If DNA origami is ever to become a practical nanotechnology for biology and biomedicine, scalable and cost-effective synthetic strategies must be developed. The employment of enzymatic reactions to synthesize scaffold and staple strands and the construction of periodic nanostructures with dramatically reduced staple strands represent two promising approaches toward this goal.

Previous efforts to construct periodic DNA nanostructures involved assembly of size-limited DNA tiles.[16,42] In the present study, we have succeeded in generating periodic DNA nanostructures using RCA-based enzymatic reactions. RCA itself produces long scaffold strands, and by integration with nicking process, it also produces short staple strands. This ultimately leads to the generation of DNA nanostructures in one pot through careful programming of the enzymatic reactions. Besides RCA, polymerase chain reaction (PCR) and nicking strand-displacement amplification (nSDA) are also commonly used DNA amplification tools. For example, Pound et al. has originally used PCR to amplify the specific segments of the genome as scaffolds.[24] However, the finite length of the replicated scaffold strands limits the final geometric size and corresponding surface area of the DNA origami nanostructures. Moreover, to reduce the cost, Marchi et al. ingeniously replaced the commercial synthetic staple strands by staple sets produced from nSDA on a chip surface.[25] However, the low amplification efficiency and the unavoidable byproducts of nSDA still restrict the applicability of this method. Compared to these two methods, the rapid production of long ssDNA from a circular template and the flexibility of template design make RCA a better tool to synthesize scaffold and staple strands for the construction of periodic DNA origami structures.

Although RCA was only used to synthesize one 96-nt staple strand for the construction of DNR in one pot, multiple staple strands would be produced simultaneously in one pool if two or more oligonucleotides are encoded into one circular template along with the proper nicking enzyme recognition sites. Therefore, DNA nanostructures requiring multiple staples could also be generated by this RCA-based enzymatic strategy. The number of staple strands could be further increased by using more than one circular template, and thereby more complex nanostructures comparable to conventional DNA origami are anticipated. If one prefers arbitrary staple strands free of sequences related to the nicking enzyme recognization sites, circular template could be designed with hairpin regions encoding restriction site.[34] However, the hairpin byproducts are generated after digestion, and the atomic economy suffers as a result. As proof of concept, here we choose the simple DNR structure which can satisfy the simplicity, cost-effectiveness, and efficiency requirements of a delivery vehicle for biomedical applications.

Although DNR is negatively charged, the distinct rigid structure with high aspect ratio and nanoscale dimension allow the insertion and penetration through the cell membranes, leading to their efficient cellular internalization. Upon entering the cells, we hypothesized that the DNRs would maintain their rigid structure and be entrapped inside the endosomes.[18] The typical size of endosomes vary from 200 nm to 1 μm, while the dimensions of DNR are in the range from 500 nm to 1.5 μm. Considering the rigidity of DNR, part of it would stretch out of one endosome, providing a mechanism for endosomal escape. The capability of DNR to escape from the endosomes endows the possibility to utilize it as a delivery vehicle for siRNA and other biologics. Combining the advantages of DNR including easy-to-modify structures, efficient endocytosis, and successful escape from endosome, DNR represents a versatile platform which holds potentials in drug delivery and elucidation of the cell physiology. We have shown two successful examples herein by demonstrating its applications in probing intracellular pH and delivering siRNA for mediating gene silencing in cancer cells.

■ ASSOCIATED CONTENT

Supporting Information

Detailed structural design, experimental methods, and characteristic data. This material is available free of charge via the Internet at http://pubs.acs.org.

■ AUTHOR INFORMATION

Corresponding Author

*yweizmann@uchicago.edu

Author Contributions

†These authors contributed equally.

Notes

The authors declare no competing financial interest.

■ ACKNOWLEDGMENTS

This research was supported by the University of Chicago. D.L. acknowledges the Martha Ann and Joseph A. Chenicek Graduate Research Fund and HHMI International Student Research Fellowship. C.H. and W.L. acknowledge funding support from NIH (U01-CA151455). AFM studies were carried out in the NSF Materials Research Science and Engineering Center (MRSEC) in University of Chicago.

■ REFERENCES

(1) Seeman, N. C. *Nature* **2003**, *421*, 427.
(2) Winfree, E.; Liu, F. R.; Wenzler, L. A.; Seeman, N. C. *Nature* **1998**, *394*, 539.
(3) Zheng, J.; Birktoft, J. J.; Chen, Y.; Wang, T.; Sha, R.; Constantinou, P. E.; Ginell, S. L.; Mao, C.; Seeman, N. C. *Nature* **2009**, *461*, 74.
(4) He, Y.; Ye, T.; Su, M.; Zhang, C.; Ribbe, A. E.; Jiang, W.; Mao, C. *Nature* **2008**, *452*, 198.
(5) Yan, H.; Park, S. H.; Finkelstein, G.; Reif, J. H.; LaBean, T. H. *Science* **2003**, *301*, 1882.
(6) Rothemund, P. W. K. *Nature* **2006**, *440*, 297.
(7) Han, D.; Pal, S.; Nangreave, J.; Deng, Z.; Liu, Y.; Yan, H. *Science* **2011**, *332*, 342.
(8) Dietz, H.; Douglas, S. M.; Shih, W. M. *Science* **2009**, *325*, 725.

DOI: 10.1021/ja512665z
J. Am. Chem. Soc. 2015, 137, 3844−3851

(9) Douglas, S. M.; Dietz, H.; Liedl, T.; Hoegberg, B.; Graf, F.; Shih, W. M. *Nature* **2009**, *459*, 414.
(10) Andersen, E. S.; Dong, M.; Nielsen, M. M.; Jahn, K.; Subramani, R.; Mamdouh, W.; Golas, M. M.; Sander, B.; Stark, H.; Oliveira, C. L. P.; Pedersen, J. S.; Birkedal, V.; Besenbacher, F.; Gothelf, K. V.; Kjems, J. *Nature* **2009**, *459*, 73.
(11) Kuzyk, A.; Schreiber, R.; Fan, Z.; Pardatscher, G.; Roller, E.-M.; Hoegele, A.; Simmel, F. C.; Govorov, A. O.; Liedl, T. *Nature* **2012**, *483*, 311.
(12) Douglas, S. M.; Bachelet, I.; Church, G. M. *Science* **2012**, *335*, 831.
(13) Gu, H.; Chao, J.; Xiao, S.-J.; Seeman, N. C. *Nature* **2010**, *465*, 202.
(14) Rinker, S.; Ke, Y.; Liu, Y.; Chhabra, R.; Yan, H. *Nat. Nanotechnol.* **2008**, *3*, 418.
(15) Wong, N. Y.; Xing, H.; Tan, L. H.; Lu, Y. *J. Am. Chem. Soc.* **2013**, *135*, 2931.
(16) Fu, Y.; Zeng, D.; Chao, J.; Jin, Y.; Zhang, Z.; Liu, H.; Li, D.; Ma, H.; Huang, Q.; Gothelf, K. V.; Fan, C. *J. Am. Chem. Soc.* **2013**, *135*, 696.
(17) He, Y.; Ye, T.; Ribbe, A. E.; Mao, C. *J. Am. Chem. Soc.* **2011**, *133*, 1742.
(18) Mei, Q.; Wei, X.; Su, F.; Liu, Y.; Youngbull, C.; Johnson, R.; Lindsay, S.; Yan, H.; Meldrum, D. *Nano Lett.* **2011**, *11*, 1477.
(19) Modi, S.; Swetha, M. G.; Goswami, D.; Gupta, G. D.; Mayor, S.; Krishnan, Y. *Nat. Nanotechnol.* **2009**, *4*, 325.
(20) Modi, S.; Nizak, C.; Surana, S.; Halder, S.; Krishnan, Y. *Nat. Nanotechnol.* **2013**, *8*, 459.
(21) Walsh, A. S.; Yin, H.; Erben, C. M.; Wood, M. J. A.; Turberfield, A. J. *ACS Nano* **2011**, *5*, 5427.
(22) Li, J.; Pei, H.; Zhu, B.; Liang, L.; Wei, M.; He, Y.; Chen, N.; Li, D.; Huang, Q.; Fan, C. *ACS Nano* **2011**, *5*, 8783.
(23) Lee, H.; Lytton-Jean, A. K. R.; Chen, Y.; Love, K. T.; Park, A. I.; Karagiannis, E. D.; Sehgal, A.; Querbes, W.; Zurenko, C. S.; Jayaraman, M.; Peng, C. G.; Charisse, K.; Borodovsky, A.; Manoharan, M.; Donahoe, J. S.; Truelove, J.; Nahrendorf, M.; Langer, R.; Anderson, D. G. *Nat. Nanotechnol.* **2012**, *7*, 389.
(24) Pound, E.; Ashton, J. R.; Becerril, H. A.; Woolley, A. T. *Nano Lett.* **2009**, *9*, 4302.
(25) Marchi, A. N.; Saaem, I.; Tian, J.; LaBean, T. H. *ACS Nano* **2013**, *7*, 903.
(26) Ma, Y.; Zheng, H.; Wang, C.; Yan, Q.; Chao, J.; Fan, C.; Xiao, S.-J. *J. Am. Chem. Soc.* **2013**, *135*, 2959.
(27) Ouyang, X.; Li, J.; Liu, H.; Zhao, B.; Yan, J.; Ma, Y.; Xiao, S.; Song, S.; Huang, Q.; Chao, J.; Fan, C. *Small* **2013**, *9*, 3082.
(28) Liu, D.; Daubendiek, S. L.; Zillman, M. A.; Ryan, K.; Kool, E. T. *J. Am. Chem. Soc.* **1996**, *118*, 1587.
(29) Geng, Y.; Dalhaimer, P.; Cai, S.; Tsai, R.; Tewari, M.; Minko, T.; Discher, D. E. *Nat. Nanotechnol.* **2007**, *2*, 249.
(30) Kam, N. W. S.; Dai, H. J. *J. Am. Chem. Soc.* **2005**, *127*, 6021.
(31) Kostarelos, K.; Lacerda, L.; Pastorin, G.; Wu, W.; Wieckowski, S.; Luangsivilay, J.; Godefroy, S.; Pantarotto, D.; Briand, J.-P.; Muller, S.; Prato, M.; Bianco, A. *Nat. Nanotechnol.* **2007**, *2*, 108.
(32) Goodman, R. P.; Schaap, I. A. T.; Tardin, C. F.; Erben, C. M.; Berry, R. M.; Schmidt, C. F.; Turberfield, A. J. *Science* **2005**, *310*, 1661.
(33) Ririe, K. M.; Rasmussen, R. P.; Wittwer, C. T. *Anal. Biochem.* **1997**, *245*, 154.
(34) Ducani, C.; Kaul, C.; Moche, M.; Shih, W. M.; Hogberg, B. *Nat. Methods* **2013**, *10*, 647.
(35) Li, H.; Park, S. H.; Reif, J. H.; LaBean, T. H.; Yan, H. *J. Am. Chem. Soc.* **2003**, *126*, 418.
(36) Lanz, E.; Gregor, M.; Slavik, J.; Kotyk, A. *J. Fluoresc.* **1997**, *7*, 317.
(37) He, C.; Lu, K.; Lin, W. *J. Am. Chem. Soc.* **2014**, *136*, 12253.
(38) Huotari, J.; Helenius, A. *EMBO J.* **2011**, *30*, 3481.
(39) Seferos, D. S.; Giljohann, D. A.; Hill, H. D.; Prigodich, A. E.; Mirkin, C. A. *J. Am. Chem. Soc.* **2007**, *129*, 15477.
(40) Altieri, D. C. *Nat. Rev. Cancer* **2008**, *8*, 61.
(41) Pennati, M.; Folini, M.; Zaffaroni, N. *Expert Opin. Ther. Targets* **2008**, *12*, 463.
(42) Zhao, Z.; Yan, H.; Liu, Y. *Angew. Chem., Int. Ed.* **2010**, *49*, 1414.

DOI: 10.1021/ja512665z
J. Am. Chem. Soc. 2015, 137, 3844−3851